

Do Topological Signatures Track Fidelity in Wind-Field Super-Resolution?

A Preliminary Study using Euler Characteristic Curves

4

January 2026

Abstract

7 Super-resolution (SR) models are commonly evaluated using pixel-based metrics
 8 such as PSNR and MSE, which quantify average intensity errors but often fail to cap-
 9 ture structural distortions that are visually or physically meaningful. In scientific sim-
 10 ulation data, such as wind fields, preserving the connectivity and organization of flow
 11 structures is often more important than minimizing per-pixel error alone.

In this work, I extend earlier topology-aware SR evaluation from natural images to two-dimensional wind-field simulation data. I compare bicubic interpolation, a convolutional neural network (CNN), and a GAN-based SR model on a medium-resolution to high-resolution (MR→HR) wind dataset. Alongside PSNR and MSE, I use Euler characteristic curves as a lightweight topological descriptor to quantify how well each method preserves the structure of wind speed and its components.

Our results reveal a consistent tradeoff: CNN-based models achieve better PSNR and MSE by producing smoother outputs, while GAN-based models preserve fine-scale structure more faithfully, leading to closer agreement with ground-truth topology despite higher pixel error. These findings suggest that topological descriptors such as Euler characteristic curves provide complementary information to pixel metrics, particularly for scientific vector-field super-resolution.

24 1 Introduction

Image super-resolution (SR) seeks to reconstruct a high-resolution signal from a lower-resolution observation. While SR has been studied extensively in the context of natural images, many emerging applications involve scientific simulation data, where the goal is not only visual fidelity but also structural and physical consistency. Examples include climate modeling, fluid dynamics, and wind-field reconstruction, where small-scale structures such as ridges, channels, and flow boundaries carry important semantic meaning.

Most SR models are evaluated using pixel-based metrics such as peak signal-to-noise ratio (PSNR) and mean squared error (MSE). These metrics measure average per-pixel

33 deviations, but they do not explicitly account for changes in structure or connectivity. As a
34 result, an SR output may score highly under PSNR while still altering the organization of
35 important features, for instance by smoothing or merging distinct regions.

36 Topological Data Analysis (TDA) provides tools for summarizing the structure of scalar
37 fields in a way that is invariant to small perturbations but sensitive to connectivity changes.
38 In earlier work, I investigated whether merge-tree-based metrics track perceptual fidelity in
39 natural image SR. In this paper, I move to a more topologically meaningful setting: wind-
40 field simulation data. Unlike natural images, wind data is inherently structured and often
41 vector-valued, making it a natural testbed for topology-aware evaluation.

42 Rather than using full merge trees, which are computationally expensive and naturally
43 defined on scalar fields, I adopt Euler characteristic curves as a lightweight 0D topological
44 descriptor. This allows us to study how SR models preserve connectivity patterns across
45 intensity thresholds while remaining computationally practical.

46 2 Problem Setting

47 I study the super-resolution of two-dimensional wind fields defined on a regular grid. Each
48 grid point has a horizontal and vertical wind component (u, v) , forming a vector field

$$\mathbf{w}(x) = (u(x), v(x)).$$

49 From these components I derive the wind speed (a scalar field)

$$s(x) = \|\mathbf{w}(x)\|_2 = \sqrt{u(x)^2 + v(x)^2},$$

50 which serves as a physically meaningful quantity for topology-aware evaluation.

51 Because merge trees and related descriptors are defined on scalar fields, I evaluate topol-
52 ogy on scalarizations of the vector field—primarily speed s —and additionally on the indi-
53 vidual components u and v to probe directional effects.

54 Given a medium-resolution (MR) input wind field x^{MR} and a corresponding high-
55 resolution ground truth x^{HR} , an SR model f_θ produces a prediction

$$\hat{x}^{\text{HR}} = f_\theta(x^{\text{MR}}).$$

56 I evaluate the prediction using:

- 57 • **Pixel-based metrics:** MSE and PSNR computed on the speed field s (and in some
58 scripts directly on the 2-channel (u, v) field; see replication notes).
- 59 • **Topological metrics:** Euler characteristic curves computed from thresholded filtra-
60 tions of s .

61 **3 Methodology**

62 **3.1 Dataset**

63 I use wind simulation data derived from the WIND Toolkit, generated using the Weather
64 Research and Forecasting (WRF) model. The data consists of spatial wind fields at multiple
65 resolutions. For this study, I focus on a medium-resolution to high-resolution (MR→HR)
66 setting.

67 Each sample consists of:

- 68 • Medium-resolution input wind field,
- 69 • High-resolution ground-truth wind field,
- 70 • Super-resolved outputs from multiple SR methods.

71 **3.2 Super-Resolution Models**

72 I evaluate three SR approaches:

- 73 1. **Bicubic interpolation** as a non-learned baseline,
- 74 2. **CNN-based SR**, optimized primarily for MSE,
- 75 3. **GAN-based SR**, optimized for perceptual realism.

76 All models operate on the same MR inputs and are evaluated against the same HR
77 ground truth.

78 **3.3 Euler Characteristic Curves**

79 Given a scalar field f , the Euler characteristic χ of a thresholded set summarizes the number
80 of connected components minus the number of holes. I compute Euler characteristic curves
81 by sweeping a threshold τ and evaluating $\chi(\tau)$ on a cubical complex induced by thresholded
82 speed fields.

83 For the main Euler curve plots in this paper (Fig. 4), I use *superlevel sets*

$$A_\tau = \{x : s(x) \geq \tau\},$$

84 8-connectivity for foreground components, and holes computed by labeling background
85 components and excluding those connected to the image boundary. Thresholds are sampled
86 from a robust GT range using the 1% and 99% quantiles of s with 80 linearly spaced values.

87 **3.4 Reproducibility and Detailed Replication Steps**

88 This section provides a complete, file-by-file procedure to reproduce all reported figures
89 and summary numbers, including required inputs, scripts to run, and expected outputs.

```
90 Prerequisites. The pipeline assumes:  
91     • Python environment with numpy, scipy, matplotlib, pandas.  
92     • The PhIREGANs codebase available on the Python path, and pretrained checkpoints  
93         present on disk.  
94     • The working directory is the project root (so relative paths resolve as written below).
```

95 **Expected directory layout.**

```
96     • Dataset TFRecords:  
97         - example_data/wind_MR-HR.tfrecord  
98             - (optional) example_data/wind_LR-MR.tfrecord  
99     • Pretrained models:  
100        - models/wind_mr-hr/trained_gan/gan  
101        - models/wind_mr-hr/trained_cnn/cnn  
102            - (optional) models/wind_lr-mr/trained_gan/gan  
103     • Output folder (created during replication):  
104         - data_out/
```

```
105 Step 0: Sanity-check the example data. This prints shapes/ranges for files under  
106 example_data/.
```

```
107  
108 python inspect_example_data.py
```

```
110 Step 1: Run paired MR→HR inference for GAN and CNN. These scripts run  
111 PhIREGANs.test_paired(...) with batch_size=1 and write numpy dumps  
112 (dataIN.npy, dataGT.npy, dataSR.npy, idx.npy) to an output directory deter-  
113 mined by PhIREGANs.
```

```
114  
115 python run_paired_wind_mr_hr.py  
116 python run_paired_wind_mr_hr_cnn.py
```

```
118 Important: downstream plotting scripts assume you collect/rename the generated out-  
119 puts into:
```

```
120     • data_out/wind_mrhr_gan/ containing: dataIN.npy, dataGT.npy,  
121         dataSR.npy, idx.npy  
122     • data_out/wind_mrhr_cnn/ containing the same four files  
123 If PhIREGANs writes to a different folder name (e.g., timestamped), copy or rename that  
124 folder to match the paths above.
```

125 **Step 2: Generate qualitative figures (triptychs + error maps).** This reads the two fold-
126 ers above and writes images to `figs_quick/`.

```
127  
128     python quick_figs.py
```

130 Expected outputs (used by Fig. 1 and Fig. 3):

- 131 • `figs_quick/error_speed.png`, `figs_quick/error_u.png`,
132 `figs_quick/error_v.png`
- 133 • `figs_quick/triptych_speed.png`, `figs_quick/triptych_u.png`,
134 `figs_quick/triptych_v.png`

135 To compile this L^AT_EX file without editing figure paths, copy these six files into the same
136 directory as the `.tex` file and rename them to: `error_speed.png`, `error_u.png`,
137 `error_v.png`, `triptych_speed.png`, `triptych_u.png`, `triptych_v.png`.
138 (Alternatively, update each `\includegraphics` path to point to `figs_quick/....`)

139 **Step 3: Generate Euler-curve plots (MR \rightarrow HR).** This script also constructs a bicu-
140 bic baseline by upsampling the MR input using `scipy.ndimage.zoom(...,`
141 `order=3)`.

```
142  
143     python plot_euler_curves_mrhr.py
```

145 Expected outputs (used by Fig. 4):

- 146 • `euler_curve_speed_mrhr.png`
- 147 • `euler_curve_abdiff_speed_mrhr.png`

148 **Step 4: Compute per-sample Euler-curve distance summaries (CSV).** This script
149 computes per-sample distances between SR and GT Euler curves and writes a CSV used
150 for bar plots.

```
151  
152     python topo_euler_eval_container.py
```

154 Expected output:

- 155 • `topo_euler_results_mrhr.csv`

156 **Step 5: Compute pixel metrics (PSNR/MSE).** Two scripts are provided:

- 157 • `all_samples_topology_psnr.py`: prints per-sample MSE/PSNR and
158 mean \pm std PSNR.
- 159 • `topology_psnr_compare.py`: prints a single global MSE/PSNR over all sam-
160 ples and both channels.

```
161  
162     python all_samples_topology_psnr.py  
163     python topology_psnr_compare.py
```

165 **Step 6: Generate summary bar plots (PSNR and topology distance).** This
166 script reads `topo_euler_results_mrhr.csv` and writes `psnr_bar.png` and
167 `chil2_bar.png`. **Note:** PSNR values are stored as a small dictionary inside the script
168 and should be updated from Step 5.

```
169 # Edit PSNR dict inside plot_metric_summary.py, then:  
170 python plot_metric_summary.py  
171
```

173 Expected outputs (used by Fig. 2):

- 174 • `psnr_bar.png`
- 175 • `chil2_bar.png`

176 **Things to note for exact replication.**

- 177 • **Output folder names:** `quick_figs.py` and
178 `plot_euler_curves_mrhr.py` assume outputs live in
179 `data_out/wind_mrhr_gan` and `data_out/wind_mrhr_cnn`. If
180 PhIREGANs writes elsewhere, copy/rename accordingly.
- 181 • **Index alignment:** `quick_figs.py` asserts `idx.npy` matches between GAN and
182 CNN runs. If indices differ, regenerate runs with consistent data ordering.
- 183 • **Bicubic baseline:** bicubic upsampling is computed via
184 `scipy.ndimage.zoom(..., order=3)` (bicubic) and applied to the
185 MR input prior to computing speed.
- 186 • **Euler curve conventions:** the main Euler-curve plots use *superlevel* sets, 8-
187 connectivity, and robust thresholds (GT 1%–99% quantiles, 80 steps). The CSV eval-
188 uation script (`topo_euler_eval_container.py`) uses a simpler implemen-
189 tation (by default sublevel sets, 4-connectivity from `scipy.ndimage.label`,
190 thresholds from min–max with 50 steps). For strict consistency across all plots/ta-
191 bles, these conventions should be unified (either by editing the script defaults or by
192 re-running with matched settings).
- 193 • **PSNR definition:** `all_samples_topology_psnr.py` computes PSNR using
194 a per-sample dynamic range derived from GT (max–min); this differs from fixed-
195 range PSNR and should be kept consistent when reporting.
- 196 • **Normalization parameters:** inference scripts pass `mu_sig` into PhIREGANs.
197 Changing these values will change both pixel metrics and topology.

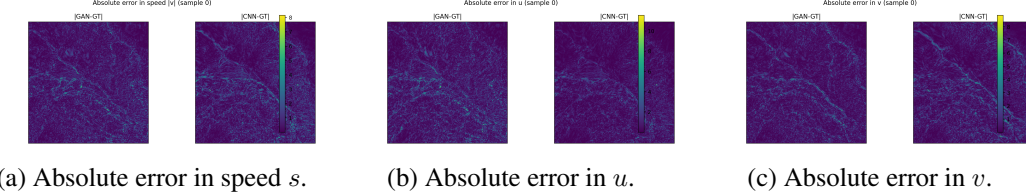


Figure 1: Per-pixel absolute error maps for sample 0. Lower values (darker) indicate closer pixel-wise agreement with the ground truth.

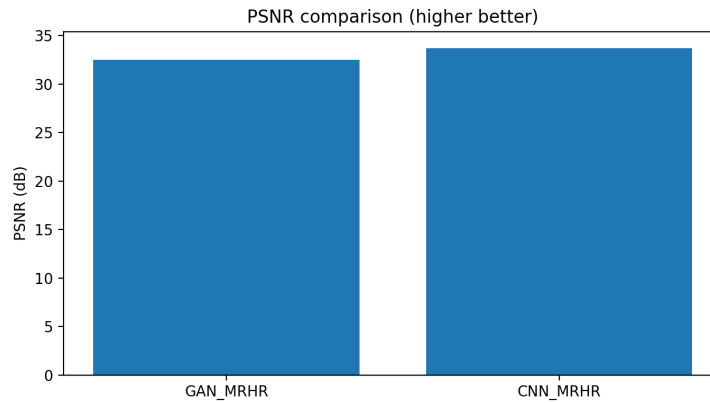


Figure 2: PSNR comparison (higher is better) for MR→HR wind SR evaluated on speed s . In this experiment, the CNN achieves higher PSNR (lower MSE), consistent with smoother predictions optimized for pixel fidelity.

198 4 Results

199 4.1 Pixel Metrics

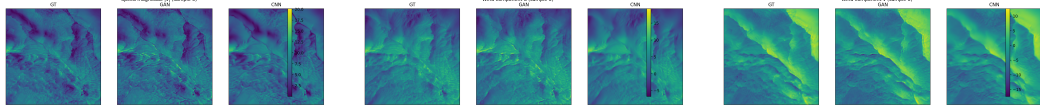
200 Across all evaluated samples, the CNN model achieves lower MSE and higher PSNR than
 201 the GAN model. This is expected, as the CNN is trained directly to minimize pixel-wise
 202 error and produces smoother outputs.

203 4.2 Qualitative Structure

204 Visual inspection reveals that the GAN preserves sharper small-scale features in the wind
 205 field, while the CNN output appears smoother and less textured. Bicubic typically under-
 206 performs learned models on both pixel metrics and qualitative structure in our experiments.

207 4.3 Topological Analysis

208 Euler characteristic curves reveal clear differences between models. CNN outputs show re-
 209 duced variability and flatter Euler curves, indicating loss of fine-scale connectivity. GAN
 210 outputs track the ground-truth Euler curves more closely across thresholds, suggesting bet-
 211 ter preservation of structural organization.



(a) Speed magnitude s (GT / GAN / CNN). (b) Wind component u (GT / GAN / CNN). (c) Wind component v (GT / GAN / CNN).

Figure 3: Qualitative comparison for MR \rightarrow HR wind super-resolution. The CNN outputs appear smoother (lower pixel error), while GAN outputs typically retain more fine-scale structure/textured that is visually closer to the HR patterns.

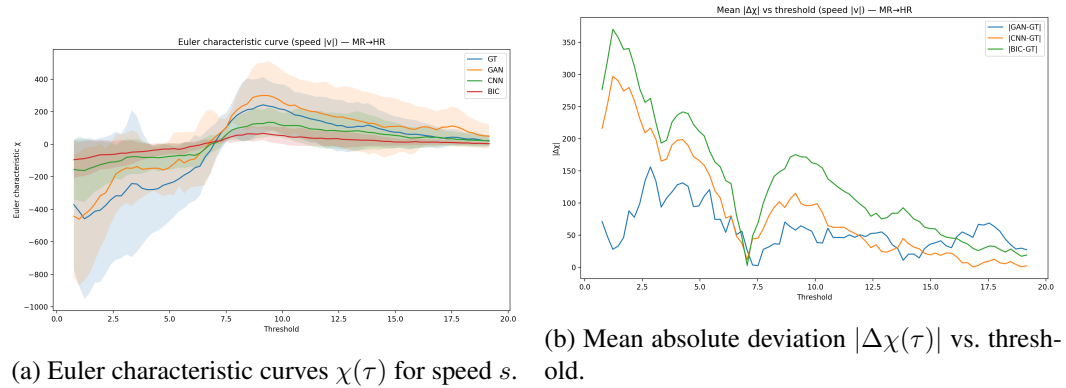


Figure 4: Topology-aware evaluation using Euler characteristic curves on thresholded wind speed s . Curves closer to GT suggest better preservation of connectivity/holes patterns across thresholds, complementing pixel metrics like PSNR.

212 Plots of mean absolute Euler curve deviation as a function of threshold further high-
213 light that topology errors concentrate at intermediate wind speeds, where small connected
214 structures are most prevalent.

215 I also observe that the threshold-wise topology error profile of the CNN closely re-
216 sembles bicubic interpolation. A plausible explanation is that both methods behave like
217 low-pass filters on the scalarized speed field: they suppress small-scale extrema and blur
218 narrow ridges, which shifts the births/merges of connected components and the filling of
219 holes to similar threshold ranges. In contrast, the GAN tends to preserve (and sometimes
220 amplify) high-frequency structure, producing a different pattern of topological deviations
221 across thresholds.

222 As a robustness check, the same analysis can be re-run with percentile-based thresholds
223 (e.g., 5th–95th percentiles per field) to reduce sensitivity to global scaling; see the replica-
224 tion scripts in Sec. 3.4.

225 5 Discussion

226 Taken together, these results illustrate a tradeoff between pixel accuracy and structural fi-
227 delity. CNN-based SR minimizes average error but smooths away fine-scale features that

228 are important for topology. GAN-based SR introduces higher pixel error but better preserves
229 connectivity patterns, as reflected in Euler characteristic curves.

230 This demonstrates that topology-aware evaluation provides information not captured by
231 PSNR or MSE alone, particularly for scientific vector-field data where structure matters.

232 **6 Limitations and Future Work**

233 This study focuses on 0D topology and scalarized wind fields. Future work will explore:

- 234 • Vector-field topology descriptors,
- 235 • Merge trees and Reeb graphs,
- 236 • Topology-aware training objectives,
- 237 • Larger datasets and temporal coherence.

238 **7 Conclusion**

239 I presented a preliminary topology-aware evaluation of wind-field super-resolution models
240 using Euler characteristic curves. Our findings suggest that pixel-based metrics alone are in-
241 sufficient for assessing structural fidelity in scientific SR tasks, and that simple topological
242 descriptors can expose meaningful differences between models. This work lays the ground-
243 work for incorporating topology more directly into the evaluation and design of scientific
244 super-resolution systems.

245 **References**